IEEE Access
Multidisciplinary | Rapid Review | Open Access Journal

Date of publication xxxx 00, 0000, date of current version xxxx 00, 0000.

Digital Object Identifier xxxx

DC-offset Compensation for Three-Phase Grid-tied SPV-DSTATCOM Under Partial Shading Condition with Improved PR Controller

AROBINDA DASH[1], (Graduate Student Member, IEEE), DURGESH PRASAD BAGARTY[1], PRAKASH KUMAR HOTA[2], RANJAN KUMAR BEHERA[3], (Senior Member, IEEE), UTKAL RANJAN MUDULI[4], (Member, IEEE), and KHALIFA AL HOSANI[4], (Senior Member, IEEE)

[1]Department of Electrical Engineering, College of Engineering and Technology, Kalinga Nagar, Ghatikia, Bhubaneswar, Odisha 751003, India (arobinda_dash@yahoo.co.in, dpbagarty@cet.edu.in)
[2]Department of Electrical Engineering, Veer Surendra Sai University of Technology, Burla, Odisha 768018, India (pkhota_ee@vssut.ac.in)
[3]Department of Electrical Engineering, IIT Patna, Patna 801103, India (e-mail: rkb@iitp.ac.in)
[4]Department of Electrical Engineering and Computer Science, Khalifa University, PO Box 127788, Abu Dhabi, UAE (utkal.muduli@ku.ac.ae, khalifa.halhosani@ku.ac.ae)

Corresponding author: Arobinda Dash, Utkal Ranjan Muduli.

This work was partly supported by Khalifa University Award No. KKJRC-2019-Trans2, Abu Dhabi, UAE.

ABSTRACT This work deals with a single-stage three-phase grid connected solar photovoltaic-distribution static compensator (SPV-DSTATCOM) under partial shading condition (PSC). During PSC, the SPV-DSTATCOM is connected with the distribution network to solve issues like active current sharing, reactive power control, and harmonic elimination. The conventional Proportional Resonant (PR) controller behaves as a notch filter at resonance frequency with high gain in magnitude, and it has very little dc-offset rejection capability. Here, an improved PR based on second-order generalized integrator (IPR-SOGI) control architecture with unity gain at the fundamental frequency and more dc-offset rejection capability has been presented to address the drawback of the PR controller. The performance of the proposed controller is examined under different loading conditions in steady-state and dynamic conditions. Finally, a comparison between the proposed controller with the PR controller and adaptive PR controller (APR). The experimental validation of the proposed prototype has been carried out in the laboratory.

INDEX TERMS Current compensation, DSTATCOM, Power quality, Proportional Resonant controller, Voltage Source Converter.

I. INTRODUCTION

IN recent years, the world pays attention to renewable energy sources due to the shortening of fossil fuel sources, air pollution, and global warming. The utilization of renewable energy sources has been promoted quickly to fulfill increasing energy demand. The distributed power generation by renewable sources has different characteristics in comparison to conventional power generation. Therefore, interdisciplinary research is going on towards developing the improvement of existing energy conversion technologies and the development of new methods in terms of novel configuration, topologies, and control techniques. Special attention is made on wide use of Solar PV (SPV) system with the grid-tied condition due to greenhouse gas effect, global warming, safety, security, and payback period [1].

The exploitation of PV systems depends on the optimization of dynamic performance, such as variation of solar radiation and robustness against various disturbances. In the specific cases of grid application, large numbers of PV panels are connected in series or parallel to synchronize with the grid. In such a system, partial shading conditions (PSC) occur due to the appearance of shadow of trees or big buildings, or stools of birds or moving clouds. In this scenario, the power versus voltage curve becomes more complex due to the appearance of multiple local maximum power points (MPP). Out of multiple local MPP, only one peak represents global

This article has been accepted for publication in a future issue of this journal, but has not been fully edited. Content may change prior to final publication. Citation information: DOI 10.1109/ACCESS.2021.3115122, IEEE Access

MPP (GMPP). The conventional technique fails to guarantee successful tracking of the GMPP and may fall in any local MPP, resulting in a significant reduction of the generated power and reducing efficiency. Recent publications show the importance of tracking GMPP under rapidly changing irradiance conditions [2], [3]. Therefore, one of the important aspects of the grid-tied PV system is harvesting maximum energy with respect to the variation of solar radiation. To search GMPP during PSC, an extreme seeking algorithm has been proposed in [1].

In a grid integrated renewable system, any small deviation of inverter output voltage and the grid voltage at PCC will lead to a high inrush current in the system. Therefore, a dedicated control action is required for grid synchronization. Phase locked loop (PLL) is the traditional choice for the researcher and industrialist for this purpose [4]. But PLL has many drawbacks such as non-linear property, complex tuning, sluggish in nature and the performance deteriorates during weak grid condition [5], [6]. To overcome these problems, many advanced tuning methods has been proposed in different literature [7]–[9]. These advanced tuning methods compete with each other in terms of computational burden, system stability, system dynamics response, improved system performance such as active current sharing with the presence of two sources, power quality issue, reactive power compensation, harmonic elimination, THD improvement of grid's current and voltage, etc. These advanced tuning methods further lead to complicated control action and reduction of the system dynamics response.

The aim of the grid-tied SPV-DSTATCOM is to inject active power and reactive power into the system with the available solar irradiation and with the absence of solar irradiation, inject harmonic compensation power required by the load termed as a distribution static synchronous compensator (DSTATCOM). This is helpful in maintaining the grid current harmonic free, sinusoidal, balanced, and unity power factor operation using current regulation. The current regulation is performed by hysteresis current regulator or linear PI regulator or predictive regulator. These classes of regulators can further be divided into the synchronous rotating d-q frame and stationary reference frame. The three-phase synchronous reference frame regulator performance is unsatisfactory, as it needs the information about phase angle in rotating frame. The controller action is erroneous if the estimation of the phase angle is not accurate. At the same time, stationary frame regulator performance is satisfactory. One of the examples of the stationary reference frame is proportional resonance (PR) controller [10]. The PR controller has been applied in active power filter [11], photovoltaic systems [12], wind turbines [13], controlled rectifiers [14], induction motor drives [15], and fuel cells [16]. The advantages of PR controller includes: 1) It offers fast dynamic and zero steady state tracking error. 2) It has very less computational burden as it does not require rotating reference frame. It is based on $\alpha\beta$ frame. 3) It is independent of PLL, but it requires a suitable synchronization algorithm

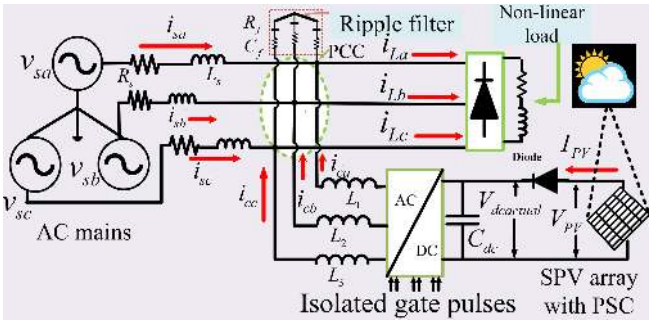

FIGURE 1. Configuration of grid integrated SPV-DSTATCOM.

for grid tie application. The disadvantage of the PR controller is that it has a high gain at the resonance frequency. The undesired anomalous peaks cause erroneous estimation for the controller. As a consequence, it leads to a significant loss of performance. Moreover, the presence of two integrators is responsible for the deviation of the frequency at which the infinite gain is located with respect to the expected resonant frequency, due to the displacement of the resonant pole. This reflects in terms of large steady-state error [17]. To overcome this one, an adaptive PR (APR) controller has been proposed in [18]. It introduces a fourth-order band pass filter and adaptive integration to detect grid frequency variation. As a consequence, it will reduce the frequency sensitivity, but it develops the complexity and computation burden of the system.

However, it is found that the estimated frequency is erroneous due to the presence of dc-offset. This causes superimposition of the low-frequency component on the average value of estimated frequency. The presence of the dc-offset not only introduces fundamental frequency oscillations, but also introduces the DC injection by the grid-tied converters. Removal of these oscillations is a very difficult task due to their low-frequency [19]. Therefore, the international standard IEC 61727 has introduced a restriction on the limitation of the dc-offset on the grid-connected photovoltaic inverters to less than 1% of their rated output current [20]. These restrictions introduce the importance of rejecting the dc-offset present in the input signal of the controller.

An improved PR controller based on SOGI (IPR-SOGI) is proposed to overcome the above issues. It not only reduces the high gain and phase jump, but also has the capability to reject the dc-offset from the input signal. The proposed controller is applied to the grid-tied SPV-DSTATCOM. The performance is validated under PSC with different loading conditions as well as dynamic conditions. It is observed to be less complex with, more dc-offset reduction capability, more harmonic elimination capability, and robust. The outstanding performance is observed by comparison of experimental results with conventional PR and APR. These are the major contributions of this work.

This paper is organized in the following five sections: section II describes the system topology and the control

This article has been accepted for publication in a future issue of this journal, but has not been fully edited. Content may change prior to final publication. Citation information: DOI 10.1109/ACCESS.2021.3115122, IEEE Access

architecture of improved PR controller; section III explains the experimental validation, and comparison result with other control structures. The conclusion is provided in section IV.

II. SPV-DSTATCOM BASED ON IPR-SOGI ALGORITHM

A. SPV-DSTATCOM SYSTEM DESCRIPTION

The schematic diagram of grid integrated three-phase three-wire SPV-DSTATCOM is shown in Fig. 1. It consists of a solar PV array, three-phase AC mains, three-phase non-linear load, three-phase VSC, interfacing inductor, and a ripple filter. The available maximum power extraction during PSC is done through the ESA method. A three-phase AC mains is connected to a three-phase non-linear load. A three-phase inductor filter is connected at the point of common coupling (PCC) to filter out high switching frequency ripples from the phase currents. The non-linear load is designed by using an uncontrolled diode bridge rectifier along with a series R-L load. At PCC, the line-line voltages are measured by using voltage sensors, and other quantities such as load side and grid side phase currents, PV voltage, and PV current, are measured and give input to the controller. A ripple filter is a series combination of resistor and capacitor, connected at PCC, for removing noise from the voltage signals.

B. CONTROL ARCHITECTURE

In this section, the extraction of the positive sequence voltage from the grid is carried out by the IPR-SOGI control algorithm. It is used to estimate the unit templates for grid synchronization. In the next step, the proposed control structure is used for the calculation of the fundamental components, which are used to estimate the reference currents for the hysteresis current controller to generate gate pulses for VSC.

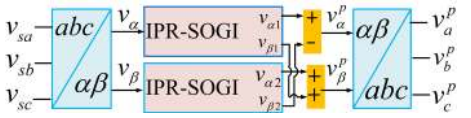

FIGURE 2. Configuration of grid integrated SPV-DSTATCOM.

C. GENERATION OF UNIT TEMPLATES

The calculation of phase voltages are calculated by sensing two line-line voltages. These phase voltages are given as follows:

$$v_{sa} = \frac{2\,v_{sab} + v_{sbc}}{3} \tag{1}$$

$$v_{sb} = \frac{v_{sbc} - v_{sab}}{3} \tag{2}$$

$$v_{sc} = \frac{-\,v_{sbc} + v_{sab}}{3} \tag{3}$$

The estimation of the balanced unit templates is carried out by extraction of the positive sequence component from the phase voltages. The phase voltages are eliminated by transferring to stationary $\alpha\beta$ -frame. The $\alpha\beta$ components are fed to the proposed controller, and the following calculation is done to generate smooth positive sequence components. It is shown in Fig. 2(a).

$$v^p_\alpha = v_{\alpha1} - v_{\beta2} \tag{4}$$

$$v^p_\beta = v_{\alpha2} + v_{\beta1} \tag{5}$$

The PCC voltages are used to find out an amplitude and in-phase (u_{pa}, u_{pb}, u_{pc}) templates as,

$$v_t = 0.816 \times \sqrt{u^2_{pa} + u^2_{pb} + u^2_{pc}} \tag{6}$$

where, v_t represents the amplitude of the terminal voltage.

$$u_{pa} = v_{pa} \times \frac{1}{v_t};\; u_{pb} = v_{pb} \times \frac{1}{v_t};\; u_{pc} = v_{pc} \times \frac{1}{v_t} \tag{7}$$

Again, the quadrature unit templates are calculated as follows:

$$u_{qa} = 0.577 \times (u_{pc} - u_{pb}) \tag{8}$$

$$u_{qb} = 0.288 \times (3u_{pa} + u_{pb} - u_{pc}) \tag{9}$$

$$u_{qc} = 0.288 \times (u_{pb} - 3u_{pa} - u_{pc}) \tag{10}$$

D. ESTIMATION OF FUNDAMENTAL COMPONENT OF LOAD CURRENT

The measured three-phase load currents consist of fundamental components, quadrature components, and harmonic components. The fundamental components represent the active power and the quadrature component represents the reactive power. In this work, the fundamental component ($\hbar_{pa}$, $\hbar_{pb}$ and $\hbar_{pc}$) and quadrature component ($\hbar_{qa}$, $\hbar_{qb}$ and $\hbar_{qc}$) of the load current of the respective phases are estimated bypassing the sensed load current through the proposed controller. The reference currents for SPV-DSTATCOM are estimated from the fundamental component of the load current. The procedure of separation of the fundamental component is shown in Fig. 3. The estimated fundamental components are passed through a sample and hold block, and it passed through a zero-crossing detector (ZCD), which are triggered by a quadrature-phase unit template corresponding to the respective phase. The average component is calculated, and it is given as,

$$\hbar_{lpa} = \frac{1}{3} \times [\hbar_{pa} + \hbar_{pb} + \hbar_{pc}] \tag{11}$$

E. ESTIMATION OF LOSS TERM

It is the extra current drawn by the capacitor to maintain the actual DC-link voltage to its reference value. This current is in phase with the supply voltage. During steady-state, the system loss is maintained by this current. It helps to maintain the DC-link voltage to its reference voltage by charging and discharging during transient state [21]. It is estimated by passing the difference of reference DC-link voltage (V_{dcref}) and actual DC-link voltage ($V_{dcactual}$) through a PI controller. It is written in discrete form as,

This article has been accepted for publication in a future issue of this journal, but has not been fully edited. Content may change prior to final publication. Citation information: DOI 10.1109/ACCESS.2021.3115122, IEEE Access

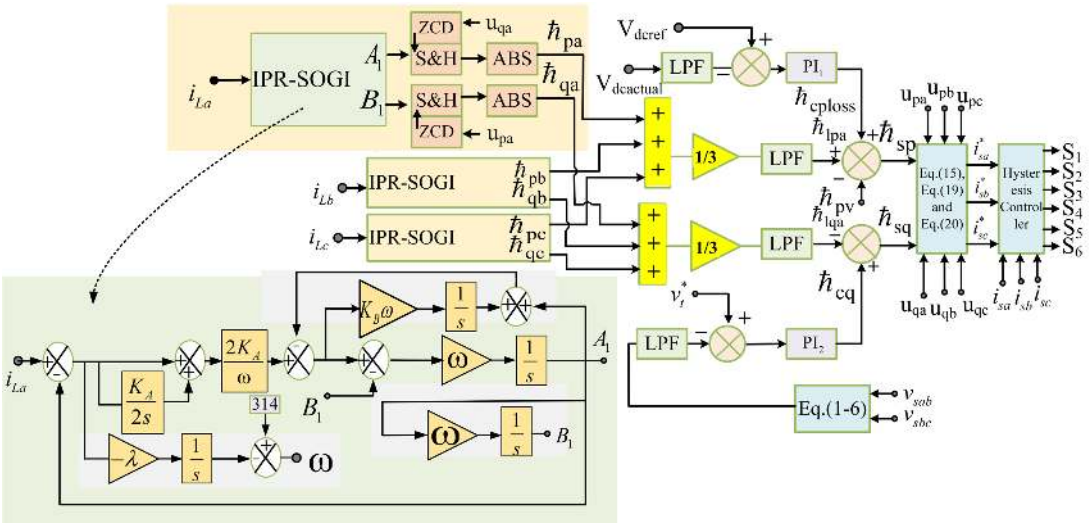

FIGURE 3. Block diagram of IPR-SOGI control algorithm for generating gate pulses.

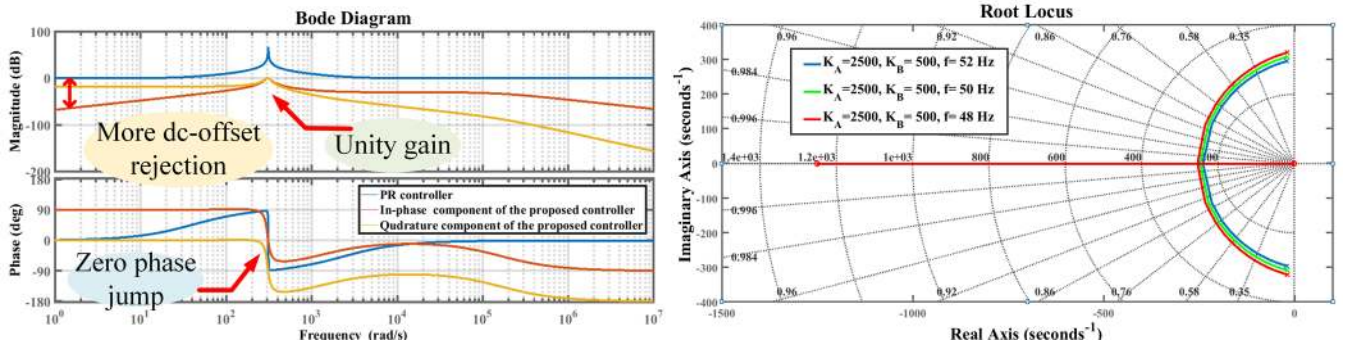

(a) (b)

FIGURE 4. Frequency response analysis: (a) comparison in between PR and IPR-SOGI (b) root locus map with variation frequency.

$$\hbar_{cploss}(i) = \hbar_{cploss}(i-1) + K_{p1}[V^*_{dc}(i) - V^*_{dc}(i-1)] + K_{i1} \times V^*_{dc}(i) \tag{12}$$

where $V^*_{dc}(i)$ $(= V_{dcref} - V_{dcactual})$ is the error in DC-link voltage. V_{dcref} can be obtained from the GMPP operation of ESA algorithm.

F. COMPUTATION OF REFERENCE CURRENT FOR CONTROLLER ACTION

A feed-forward term $\hbar_{pv}$ of SPV is estimated as,

$$\hbar_{pv} = \frac{2}{3}\frac{V_{PV} \times I_{PV}}{v_t} \tag{13}$$

The loss component and average load active components are supplied by the grid.

$$\hbar_{sp} = \hbar_{lpa} + \hbar_{cploss} - \hbar_{pv} \tag{14}$$

The fundamental reference currents are generated by multiplying the net component with corresponding unit templates as follows:

$$i^*_{pa} = \hbar_{sp} \times U_{pa}; \tag{15}$$

$$i^*_{pb} = \hbar_{sp} \times U_{pb}; \tag{16}$$

$$i^*_{pc} = \hbar_{sp} \times U_{pc} \tag{17}$$

For zero voltage regulation (ZVR), the reactive reference current can be found out from the voltage control loop with PI controller output. The steps are provided as follows:

$$v_{terror}(i) = v^*_t(i) - v_t(i) \tag{18}$$

where $v^*_t(i)$ is calculated (7) and $v_t(i)$ is the measured value.

$$\hbar_{cq}(i) = \hbar_{cq}(i-1) + K_{p2}[v_{terror}(i) - v_{terror}(i-1)] + K_{i2} \times v_{terror}(i) \tag{19}$$

The reactive weight component is estimated by the difference between the average reactive weight of the fundamental component and the AC loss component, i.e.,

$$\hbar_{sq} = \hbar_{cq} - \hbar_{lqa} \tag{20}$$

This article has been accepted for publication in a future issue of this journal, but has not been fully edited. Content may change prior to final publication. Citation information: DOI 10.1109/ACCESS.2021.3115122, IEEE Access

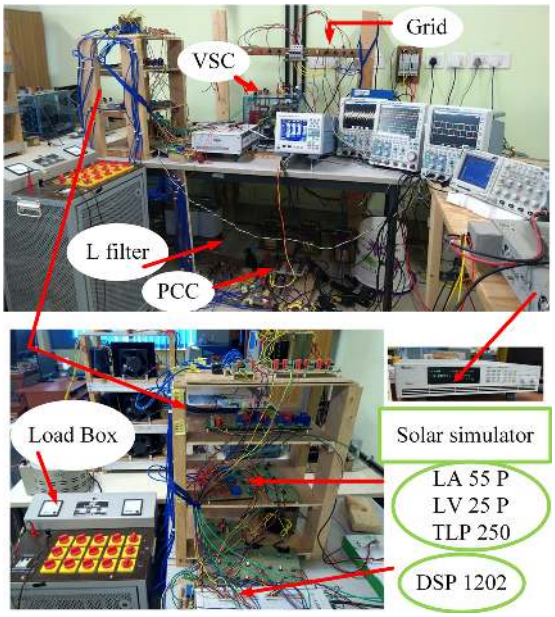

FIGURE 5. Experiment set-up developed at laboratory.

TABLE 1. Experimental set-up parameters

System quantities	Values
Source voltage (rms)	39.28 V, 38.54 V, 48.86 V L-N, 50 Hz
Feeder impedance	R_s = 0.3 Ω, L_s = 0.03 mH, R_s/X_s = 3.185
Ripple filter	R_f = 6 Ω, C_f = 10 μF
Non-linear load	3-Φ rectifier with RL load of 4 Ω, 40 mH
Load power	$P_L = 1.49kW, Q_L = 309Var$
Load current	12.59 A
PI tuning parameter	K_{p1} = 0.152, K_{i1} = 0.016, K_{p2} = 0.0136, K_{i2} = 0.0019
DSTATCOM parameter	V_{dc}^* = 150 V, C_{dc} = 2200 μF, L_f = 5 mH
PV emulator rating	P_{mpp} = 741 W, V_{GMPP} = 110.4 V, I_{GMPP} = 6.7 A, V_{pv} = 111.27 V, I_{pv} = 6.64 A

where $\hbar_{lqa} = \frac{1}{3} \times [\hbar_{qa} + \hbar_{qb} + \hbar_{qc}]$. The reactive weight component is estimated as,

$$i_{qa}^* = U_{qa} \times \hbar_{sq}; \tag{21}$$
$$i_{qb}^* = U_{qb} \times \hbar_{sq}; \tag{22}$$
$$i_{qc}^* = U_{qc} \times \hbar_{sq} \tag{23}$$

Finally, the reference grid currents are estimated as,

$$i_{sa}^* = i_{pa}^* + i_{qa}^*; \tag{24}$$
$$i_{sb}^* = i_{pb}^* + i_{qb}^*; \tag{25}$$
$$i_{sc}^* = i_{pc}^* + i_{qc}^* \tag{26}$$

The error is generated by the reduction of the sensed grid currents (i_{sa}, i_{sb}, i_{sc}) from grid reference currents ($i_{sa}^*, i_{sb}^*, i_{sc}^*$). These errors are passed through the hysteresis current controller to generate gate pulses. The hysteresis bandwidth is taken as 0.05 A. From Fig. 3, the transfer function of the proposed controller (in-phase signal, A_1 and input signal,i_{La}) and (quadrature signal, B_1 and input signal,i_{La}) are as follows:

$$\frac{A_1}{i_{La}} = \frac{2K_A s^2 + K_A^2 s}{s^3 + (2K_A + K_B\omega + \omega)s^2 + (\omega^2 + K_A^2)s + K_B\omega^3} \tag{27}$$

$$\frac{B_1}{i_{La}} = \frac{2K_A\omega s + K_A^2\omega}{s^3 + (2K_A + K_A\omega + \omega)s^2 + (\omega^2 + K_A^2)s + K_B\omega^3} \tag{28}$$

Fig. 4(a) shows the Bode plot of the proposed control structure in comparison to the conventional PR controller. Here, it is observed that the proposed controller acts as a bandpass filter and has better dc-offset rejection capability in comparison to PR controller. The PR controller acts as a notch filter and has a flat character in the magnitude plot. However, the proposed controller has zero phase jump in comparison to the conventional controller. It is observed that both phase margin and gain margin are positive, which represents the proposed controller is stable. From the Bode plot, it is found that the system is more stable at K_A = 2500 and K_B=500. The stability of the proposed controller with the variation of grid frequency (f) during transient conditions is shown in Fig. 4(b).

III. EXPERIMENTAL VERIFICATION

An experimental prototype of grid-tied SPV-DSTATCOM is developed in the laboratory for testing the proposed control algorithm. It is shown in Fig. 5. It consists of a solar PV simulator (Chroma 62020H-150S), three-phase two-level VSC, interfacing inductors, a combination of three-phase diode bridge rectifier with R-L load as a non-linear load. The control algorithm is implemented by using Digital Signal Processor (dSPACE 1102). The Hall effect voltage (LEM LV 25P) and current (LEM 55P) transducers for sensing the voltage and current signal used in developing the experimental prototype. A four-channel YOKOGAWA WT500 power analyzer and a four-channel YOKOGAWA DSO-DLM2024 digital storage oscilloscope have been used for the recording of steady-state and transient waveforms. Generated pulses are passed through the TLP-250 circuit for isolation purposes and are fed to the VSC. The DC-link reference voltage is estimated from the ESA algorithm. During the test, the DC-link voltage is operated at the GMPP voltage of the SPV (V_{mpp}). Here, V_{mpp} is 110.4 V. The experimental parameters of the grid integrated SPV-DSTATCOM system is given in

This article has been accepted for publication in a future issue of this journal, but has not been fully edited. Content may change prior to final publication. Citation information: DOI 10.1109/ACCESS.2021.3115122, IEEE Access

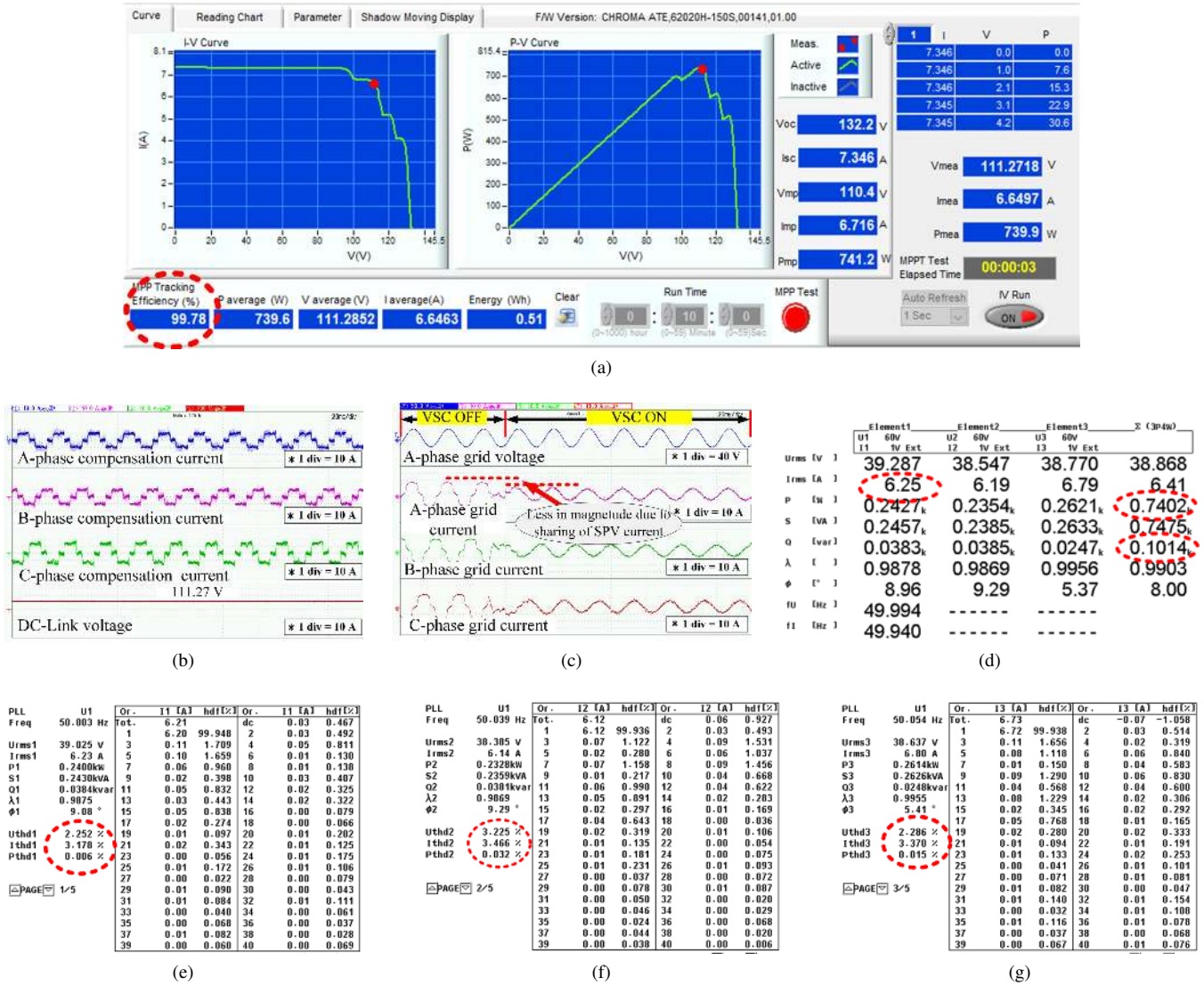

(a) (b) (c) (d) (e) (f) (g)

FIGURE 6. Steady-state performance validation with PSC under balance grid and balance non-linear loading: (a) GMPP response of SPV-DSTATCOM at $1000W/m^2$, (b) A-phase compensation current (i_{ca}), B-phase compensation current (i_{cb}), C-phase compensation current (i_{cc}) and DC-link voltage ($V_{dcactual}$), (c) line-line voltage (v_{sab}), A-phase grid current (i_{sa}), B-phase grid current (i_{sb}) and C-phase grid current (i_{sc}), (d) power quality analysis after compensation, (e) THD of A-phase grid current, (f) THD of B-phase grid current, (g) THD of C-phase grid current.

TABLE-I.

A. STEADY-STATE PERFORMANCE ANALYSIS WITH PSC

The prototype is tested with PSC under a balanced grid and a non-linear loading condition. The shadow is developed with help of a solar simulator. This leads to generates of multiple humps in the current vs voltage characteristics curve of SPV. This also leads to developing multiple local MPP on the power curve of SPV. It is shown in Fig. 6(a). Under PSC the magnitude of the SPV voltage is 110.4 V and the current is 6.64 A. The SPV is operating at 99.78% efficiency with respect to available power (741 W), which shows the maximum energy is being harvested from the solar array. Fig. 6(b) represents the compensation currents (i_{ca}, i_{cb} and i_{cc}) drawn from the VSC and the DC-link voltage ($V_{dcactual}$) is maintained with its reference value generated from the GMPP operation. Fig. 6(c) shows the line-line voltage of the grid (v_{sab}) and grid currents (i_{sa}, i_{sb} and i_{sc}). Here, initially, the grid is providing non-linear characteristics of the current to the load as per the demand of the load. With the operation of the SPV-DSTATCOM, the grid current becomes sinusoidal and having less in magnitude due to sharing of MPP current from SPV. Fig. 6(d) represents the power quality analysis of the system on the grid side. Initially, the grid is providing 1.4 kW active power and 309 VAR reactive power to the load. The load is drawing 12.5 A current in all three phases. With the operation of the SPV-DSTATCOM, the grid current magnitude decreases to 6.25 A, whereas active power decreases to 740 W and reactive power decreases to 101 Vars. The %THD of grid currents are shown in Figs. 6(e)-(g).

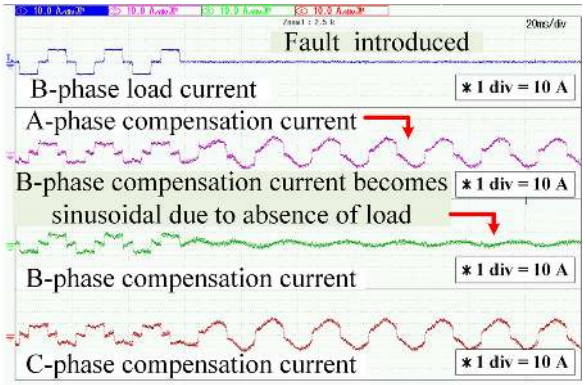

(a)

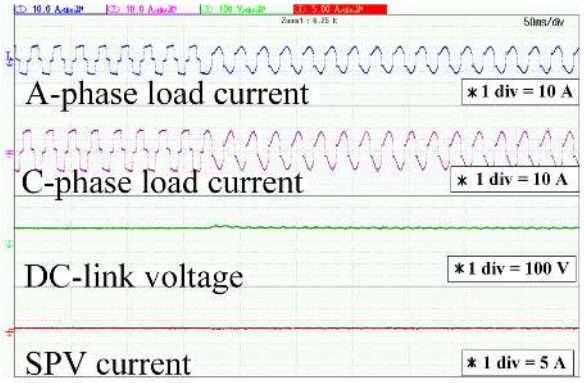

(b)

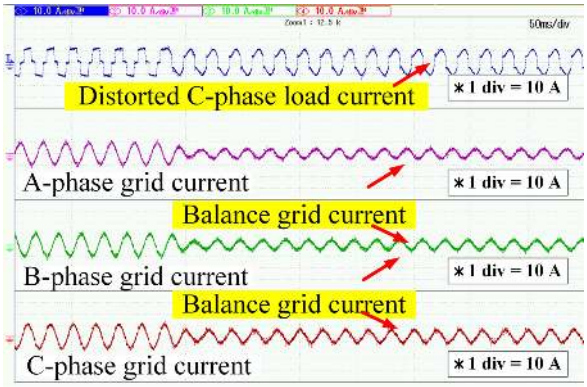

(c)

FIGURE 7. Transient-state performance validation with PSC under balance grid and unbalance loading: (a) B-phase load current (i_{Lb}), A-phase compensation current (i_{ca},), B-phase compensation current (i_{cb}) and C-phase compensation current (i_{cc}), (b) A-phase load current (i_{La}), C-phase load current (i_{Lc}), DC-link voltage ($V_{dcactual}$) and SPV current (I_{pv}), (c) C-phase load current (i_{Lb}), A-phase grid current (i_{sa}), B-phase grid current (i_{sb}) and C-phase grid current (i_{sc}).

B. TRANSIENT STATE PERFORMANCE WITH UNBALANCE LOADING UNDER PSC

Figs. 7(a)-(c) depicted the dynamic response of SPV-DSTATCOM under perturbation of B-phase load. With the rejection of the B-phase load, the net harmonic current required by the load is reduced, thus the output of the B-phase of the SPV-DSTATCOM is reduced. It is demonstrated in Fig. 7(a). Fig. 7(b) represents the nature load currents of the A-phase and C-phase. It also ensures stable operation with constant DC-link voltage and constant MPP current during the transient condition. Fig. 7(c) represents the response grid currents under this scenario. As the demand of the load reduces, the grid current magnitude decreases, and it remains sinusoidal due to compensation action performed by SPV-DSTATCOM.

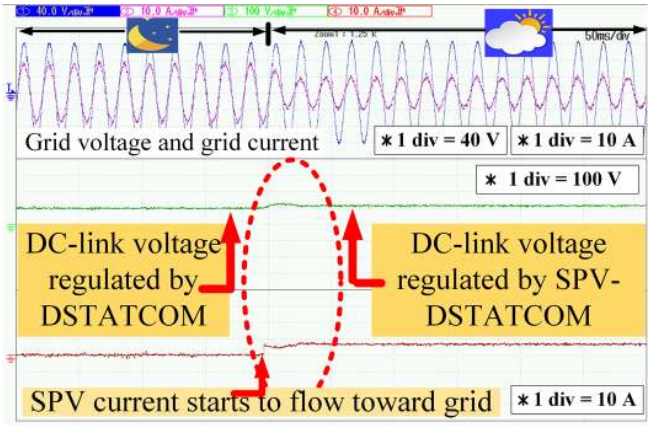

(a)

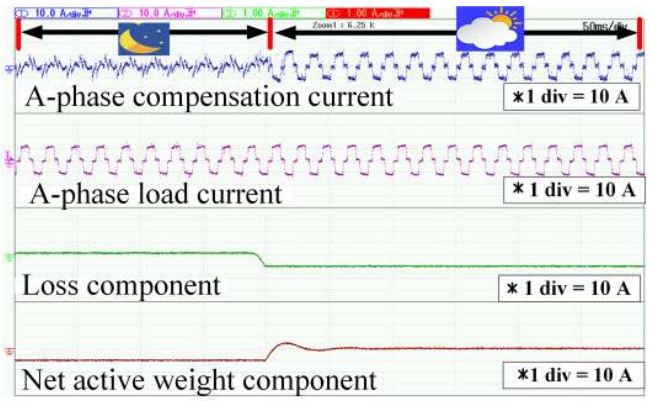

(b)

FIGURE 8. Dynamic condition analysis under PSC with change over from night mode to day mode: (a) A-phase grid voltage (v_{sa}), A-phase grid current (i_{sa}), DC-link voltage ($V_{dcactual}$) and SPV current (I_{pv}), (b) A-phase compensation current (i_{ca},), A-phase load current (i_{La}), loss component ($\hbar_{cploss}$) and net active weight current component ($\hbar_{sp}$).

C. NIGHT MODE TO DAY MODE

Fig. 8(a) represents the operation of SPV-DSTATCOM from night mode to day mode. With the absence of solar radiation, the SPV-DSTATCOM operates in DSTATCOM mode with DC-link voltage of 105 V and SPV current at 0 A. With the availability of solar radiation, SPV current increases from 0 A to 6.64 A, DC-link voltage maintained at V_{mpp} (110 V), grid current magnitude decreases, and in-phase with the grid voltage. Fig. 8(b) represents the A-phase compensation current flow from the VSC, A-phase load current, loss component, and net active weight component. Initially, the compensation current contains the harmonic current required by the load

This article has been accepted for publication in a future issue of this journal, but has not been fully edited. Content may change prior to final publication. Citation information: DOI 10.1109/ACCESS.2021.3115122, IEEE Access

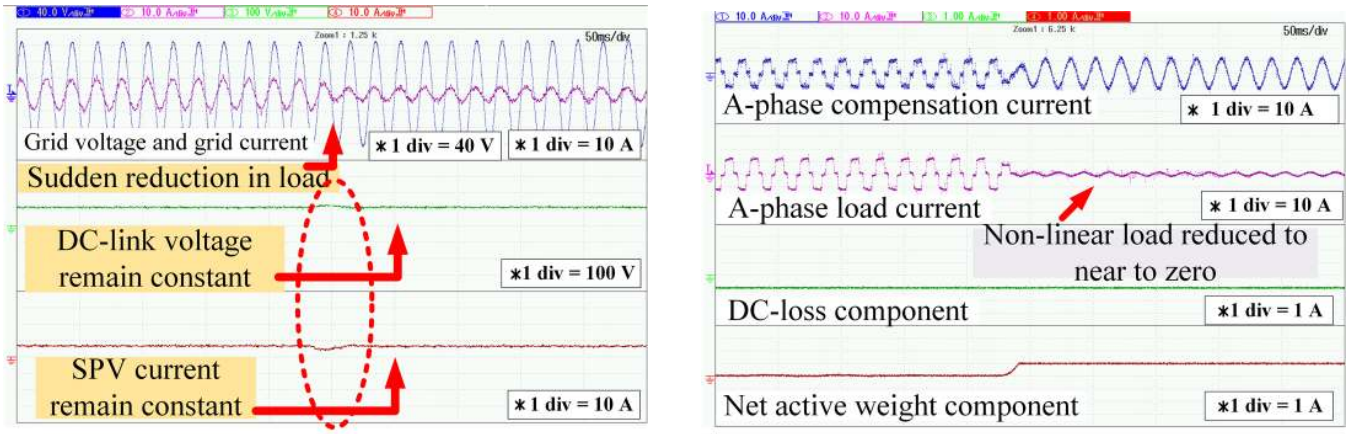

(a) (b)

FIGURE 9. Dynamic condition analysis with PSC under sudden reduction of load demand (a) A-phase grid voltage (v_{sa}), A-phase grid current (i_{sa}), DC-link voltage ($V_{dcactual}$) and SPV current (I_{pv}) (b) A-phase compensation current (i_{ca}), A-phase load current (i_{La}), loss component ($\hbar_{cploss}$) and net active weight current component ($\hbar_{sp}$).

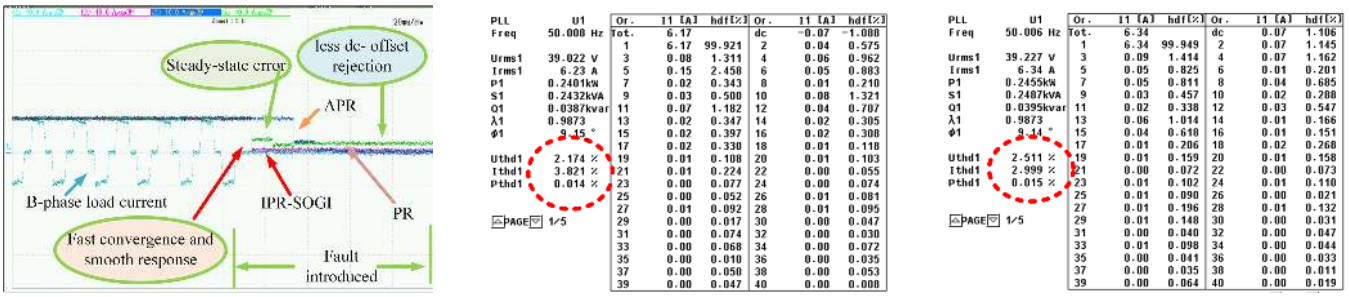

(a) (b) (c)

FIGURE 10. Comparison between IPR-SOGI, PR and APR: (a) dynamic response weight component with B-phase load disconnection, at steady state, (b) A-phase grid current THD for PR, (c) A-phase grid current THD for APR.

(act as DSTATCOM) with the availability of solar radiation it delivers active current which is in phase with the grid voltage.

D. SUDDEN REDUCTION OF LOAD WITH PSC

Initially, the SPV-DSTATCOM operates at its full load capacity. The load current is shared between the grid and SPV as per the availability of solar radiation. With sudden decreases in load, the extra power generated by the SPV will deliver to the grid. It is shown in Fig. 9(a). Here, the grid voltage and grid current are in phase, at full load capacity and sudden reduction of load it becomes out-of-phase. The DC-link voltage and SPV current remain constant with their previous value. From Fig. 9(b) it is observed that the loss component ($\hbar_{cploss}$) remains as it is due to no changes occurring in DC-link voltage. With the reduction of the grid current, the net active weight current component ($\hbar_{sp}$) increases.

E. COMPARISON RESULT

A comparison between the proposed controller with PR and APR dynamic response of weight component with respect to the removal of load is shown in Fig. 10(a). It is observed that the proposed controller has fast convergence, less steady-state error, more dc-offset rejection capability, and quick response in comparison to the other controllers. Fig. 10(b) represents the THD of A-phase grid current with PR and Fig. 10(c) represents THD of A-phase of grid current with APR controller at steady-state respectively. With close observation, it is found that the proposed controller has less THD

TABLE 2. Comparative Analysis

Algorithm	Grid current THD	Dc-offset rejection	Steady state error	PSC
PR [10]	3.82%	no rejection	moderate	no
APR [18]	2.9%	less rejection capability	slow	no
Proposed	3.1%	more rejection capability	quick response	yes

in grid current in comparison to PR and APR. The overall comparison results are shown in Table II.

IV. CONCLUSION

The real-time implementation of grid integrated SPV-DSTATCOM at PSC with an objective of dc-offset rejection has been demonstrated. The available maximum power has been harvested from the SPV-DSTATCOM under different dynamic conditions by using the ESA algorithm. From the obtained result, it is observed that the power quality of the grid is improved at erratic SPV energy production and abnormal circumstances at the grid side as well as at the load side. Excellent performance has been noticed for the IPR-SOGI algorithm in comparison to the conventional PR filter. Experiments are conducted on the prototype developed in the laboratory, and test results have verified the operation of the system to be acceptable.

.

APPENDIX A GMPP TRACKING AND DC-LINK REFERENCE VOLTAGE GENERATION

- Initialize all voltages corresponding to humps occurs in the power vs voltage characteristics curve of the SPV.
- Apply ESC for iteration process of each initialized voltages. These voltages approaching their local MPP. Store the Local MPPT with respect to their voltages.
- Compute P_m, P_n, $\frac{P_m}{V_m}$ and $\frac{P_n}{V_n}$ where m= 1,2,3,4 and n= 1,2,3,4 and m $\neq$ n.
- If $P_m > P_n$ and $\frac{P_m}{V_m} > \frac{P_n}{V_n}$ satisfied, eliminate V_n from the next iteration. Repeat the total process until unless one GMPP is tracked and find the corresponding voltage as V_{dcref}.

REFERENCES

[1] A. I. Bratcu, I. Munteanu, S. Bacha, D. Picault, and B. Raison, "Cascaded dc–dc converter photovoltaic systems: Power optimization issues," *IEEE Transactions on Industrial Electronics*, vol. 58, no. 2, pp. 403–411, 2010.

[2] I. R. Balasubramanian, S. I. Ganesan, and N. Chilakapati, "Impact of partial shading on the output power of pv systems under partial shading conditions," *IET power Electronics*, vol. 7, no. 3, pp. 657–666, 2013.

[3] K. Sundareswaran, S. Peddapati, and S. Palani, "Application of random search method for maximum power point tracking in partially shaded photovoltaic systems," *IET Renewable Power Generation*, vol. 8, no. 6, pp. 670–678, 2014.

[4] C. Zhang, X. Zhao, X. Wang, X. Chai, Z. Zhang, and X. Guo, "A grid synchronization pll method based on mixed second-and third-order generalized integrator for dc offset elimination and frequency adaptability," *IEEE Journal of Emerging and Selected Topics in Power Electronics*, vol. 6, no. 3, pp. 1517–1526, 2018.

[5] X. He, H. Geng, and S. Ma, "Transient stability analysis of grid-tied converters considering pll's nonlinearity," *CPSS Transactions on Power Electronics and Applications*, vol. 4, no. 1, pp. 40–49, 2019.

[6] S. Sahoo, S. Prakash, and S. Mishra, "Power quality improvement of grid-connected dc microgrids using repetitive learning-based pll under abnormal grid conditions," *IEEE Transactions on Industry Applications*, vol. 54, no. 1, pp. 82–90, 2017.

[7] M. Karimi-Ghartemani, S. A. Khajehoddin, P. K. Jain, A. Bakhshai, and M. Mojiri, "Addressing dc component in pll and notch filter algorithms," *IEEE Transactions on Power Electronics*, vol. 27, no. 1, pp. 78–86, 2011.

[8] W. Li, X. Ruan, C. Bao, D. Pan, and X. Wang, "Grid synchronization systems of three-phase grid-connected power converters: A complex-vector-filter perspective," *IEEE Transactions on Industrial Electronics*, vol. 61, no. 4, pp. 1855–1870, 2013.

[9] J. Matas, M. Castilla, J. Miret, L. G. de Vicuña, and R. Guzman, "An adaptive prefiltering method to improve the speed/accuracy tradeoff of voltage sequence detection methods under adverse grid conditions," *IEEE Transactions on Industrial Electronics*, vol. 61, no. 5, pp. 2139–2151, 2013.

[10] M. Cespedes and J. Sun, "Adaptive control of grid-connected inverters based on online grid impedance measurements," *IEEE Transactions on sustainable energy*, vol. 5, no. 2, pp. 516–523, 2014.

[11] C. Lascu, L. Asiminoaei, I. Boldea, and F. Blaabjerg, "High performance current controller for selective harmonic compensation in active power filters," *IEEE Transactions on Power electronics*, vol. 22, no. 5, pp. 1826–1835, 2007.

[12] R. Teodorescu, F. Blaabjerg, U. Borup, and M. Liserre, "A new control structure for grid-connected lcl pv inverters with zero steady-state error and selective harmonic compensation," in *Nineteenth Annual IEEE Applied Power Electronics Conference and Exposition, 2004. APEC'04.*, vol. 1. IEEE, 2004, pp. 580–586.

[13] P. Zhou, Y. He, and D. Sun, "Improved direct power control of a dfig-based wind turbine during network unbalance," *IEEE Transactions on Power Electronics*, vol. 24, no. 11, pp. 2465–2474, 2009.

[14] D. Roiu, R. I. Bojoi, L. R. Limongi, and A. Tenconi, "New stationary frame control scheme for three-phase pwm rectifiers under unbalanced voltage dips conditions," *IEEE Transactions on Industry Applications*, vol. 46, no. 1, pp. 268–277, 2009.

[15] R. Bojoi, E. Levi, F. Farina, A. Tenconi, and F. Profumo, "Dual three-phase induction motor drive with digital current control in the stationary reference frame," *IEE Proceedings-Electric Power Applications*, vol. 153, no. 1, pp. 129–139, 2006.

[16] S.-Y. Park, C.-L. Chen, J.-S. Lai, and S.-R. Moon, "Admittance compensation in current loop control for a grid-tie lcl fuel cell inverter," *IEEE Transactions on Power Electronics*, vol. 23, no. 4, pp. 1716–1723, 2008.

[17] R. Bojoi, L. R. Limongi, F. Profumo, D. Roiu, and A. Tenconi, "Analysis of current controllers for active power filters using selective harmonic compensation schemes," *IEEJ Transactions on electrical and electronic engineering*, vol. 4, no. 2, pp. 139–157, 2009.

[18] H. Khalfalla, S. Ethni, M. Al-Greer, V. Pickert, M. Armstrong *et al.*, "An adaptive proportional resonant controller for single phase pv grid connected inverter based on band-pass filter technique," in *2017 11th IEEE International Conference on Compatibility, Power Electronics and Power Engineering (CPE-POWERENG)*. IEEE, 2017, pp. 436–441.

[19] S. Golestan, J. M. Guerrero, and G. B. Gharehpetian, "Five approaches to deal with problem of dc offset in phase-locked loop algorithms: Design considerations and performance evaluations," *IEEE Transactions on Power Electronics*, vol. 31, no. 1, pp. 648–661, 2015.

[20] I. E. Commission *et al.*, "Photovoltaic (pv) systems-characteristics of the utility interface," *IEC Stand*, vol. 61727, 2004.

[21] A. Bhattacharya and C. Chakraborty, "A shunt active power filter with enhanced performance using ann-based predictive and adaptive controllers," *IEEE transactions on industrial electronics*, vol. 58, no. 2, pp. 421–428, 2010.